American Mineralogist, Volume 65, pages 540–556, 1980

Phase relations and their petrological implications in the system MgO–SiO_2–H_2O–CO_2 at pressures up to 100 kbar

DAVID E. ELLIS[1] AND PETER J. WYLLIE

Department of Geophysical Sciences, University of Chicago
Chicago, Illinois 60637

Abstract

A comprehensive model has been developed for phase relations in the system MgO–SiO_2–H_2O–CO_2 on the basis of Schreinemakers' rules and subsolidus thermodynamic data. The assemblage forsterite plus enstatite can melt in the presence of vapor of any H_2O/CO_2 ratio at low pressures, in the presence of vapor whose H_2O/CO_2 ratio is buffered by magnesite at intermediate pressures, and at a vapor-absent eutectic at high pressures. Forsterite and H_2O–CO_2 vapor cannot coexist at pressures greater than 90 kbar. A thermal maximum is postulated to exist on the reaction Fo + En + V → L at pressures greater than 35 kbar. Thermal maxima on vapor-present melting reactions may be responsible for the eruption of kimberlitic magma from the upper mantle.

Introduction

H_2O and CO_2 are the most abundant volatile compounds in the earth's crust. It is now apparent that they also play important roles in upper mantle processes, although their abundance in the mantle is apparently low. Subsolidus reactions involving small amounts of carbonates and hydrates plus the silicate minerals of the earth's upper mantle can buffer the composition of the vapor phase, as reviewed by Wyllie (1978) and Eggler (1978). The thermodynamic basis for such buffering has been reviewed for reactions occurring at lower pressures by Greenwood (1962, 1967), Kerrick (1974), and Kerrick and Slaughter (1976).

Eggler (1975) reported on experimental studies in the system MgO–SiO_2–H_2O–CO_2 at 20 kbar. Mysen and Boettcher (1975a,b) have discussed experimental results on the effects of H_2O, CO_2, and H_2O–CO_2 mixtures on the melting of peridotite at 20 kbar. The effects of H_2O, CO_2, and H_2O–CO_2 mixtures on the phase relationships of peridotites have been investigated in several laboratories, with emphasis on melting relationships at pressures up to 35 kbar (Brey and Green, 1975, 1976; Eggler, 1974, 1976a, 1978; Mysen and Boettcher, 1975a,b; Wyllie and Huang, 1975, 1976). Differences in experimental results and interpretations have been extensively discussed (Eggler, 1976b; Green, 1976; Mysen and Boettcher, 1975a,b; Nehru and Wyllie, 1975; Wyllie, 1978; Wyllie and Huang, 1975, 1976).

Phase relations in the system MgO–SiO_2–H_2O–CO_2 are a fundamental part of the model mantle system CaO–MgO–Al_2O_3–SiO_2–H_2O–CO_2 and understanding them is an essential step in progress toward full understanding of melting and crystallization processes in the upper mantle. Phase relations in the simple systems MgO–SiO_2–CO_2, MgO–H_2O–CO_2, and MgO–SiO_2–H_2O have been modeled, respectively, by Wyllie and Huang (1976), Ellis and Wyllie (1979a), and Ellis and Wyllie (1979b). We have used those models plus calculations of subsolidus and melting relations whenever possible to derive a model for the system MgO–SiO_2–H_2O–CO_2. Compositions in the system MgO–SiO_2–H_2O–CO_2 are clearly different from those of the earth's upper mantle. However, the system contains olivine, pyroxene, hydrate, carbonate, vapor, and liquid. It therefore indicates the general features of phase relationships possible between those types of compounds in the upper mantle.

In this paper phases in the system MgO–SiO_2–H_2O–CO_2 will be referred to by using the names of corresponding minerals. The following abbreviations for mineral names have been used to write reactions

[1] Present address: Conoco Inc., Research and Development Department, Exploration Research Division, P. O. Box 1267, Ponca City, Oklahoma 74601.

0003–004X/80/0506–0540$02.00

and to label all figures: periclase (MgO) = Pe, magnesite ($MgCO_3$) = MC, brucite [$Mg(OH)_2$] = Br, polymorphs of silica (SiO_2) = Q, enstatite ($MgSiO_3$) = En, forsterite (Mg_2SiO_4) = Fo, liquid = L, pure H_2O vapor = H_2O, pure CO_2 vapor = CO_2, and mixed H_2O–CO_2 vapor = V.

The bounding ternary systems

The framework for this study is given by the univariant curves for ternary and quaternary reactions in Figure 1. Invariant points are identified by parentheses enclosing the crystalline phases that are not present: three phases for ternary points and two phases for quaternary points. Ternary and quaternary reactions involve four and five phases, respectively. Only reactions with free vapor are plotted; some vapor-absent reactions are indicated by short lines from invariant points.

SiO_2–H_2O–CO_2

The system SiO_2–H_2O was investigated by Kennedy *et al.* (1962) at pressures up to 9.5 kbar. A criti-

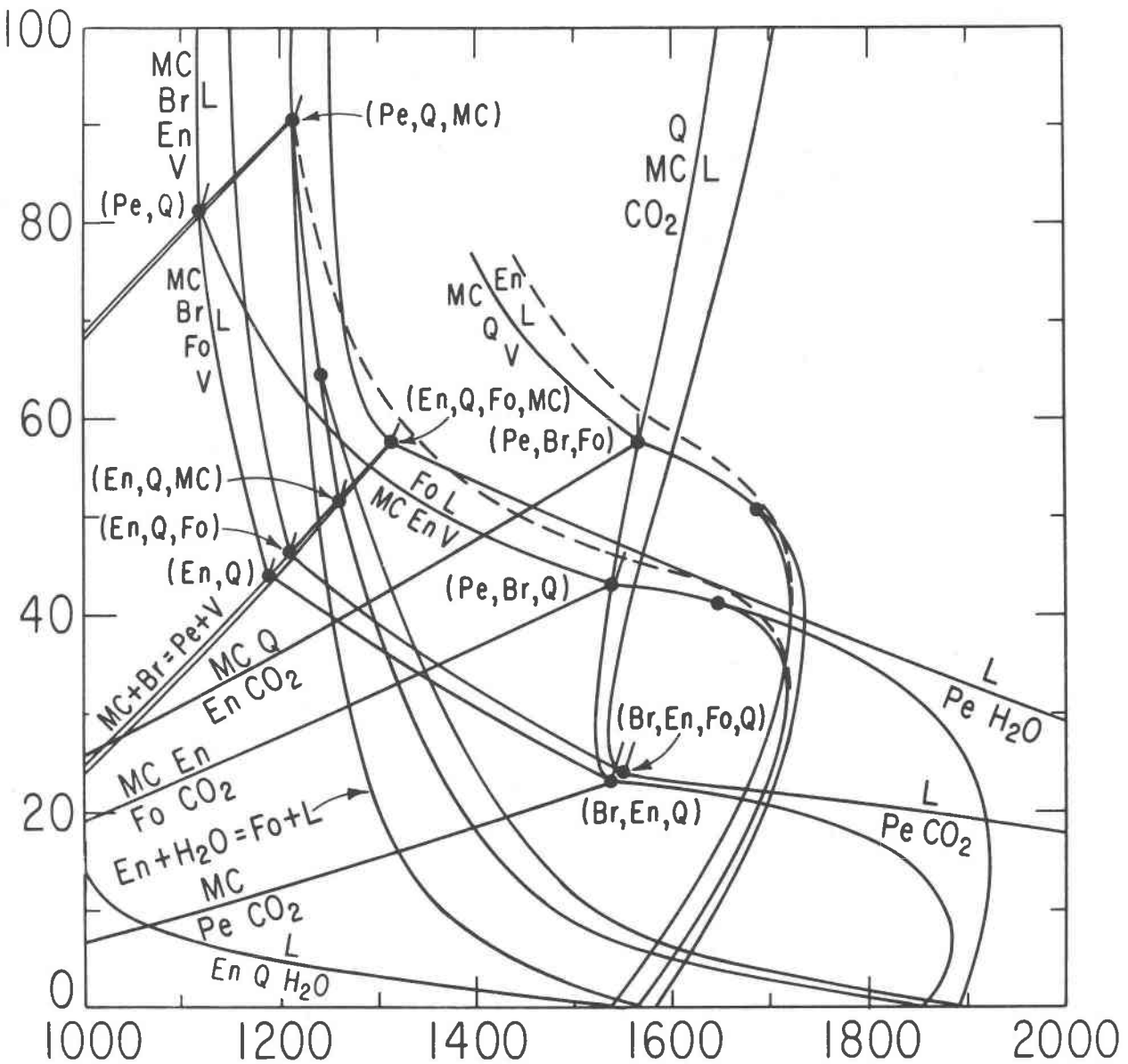

Fig. 1. Schematic *P–T* net showing subsolidus and melting reactions in the system MgO–SiO_2–H_2O–CO_2. Only vapor-present reactions are shown. Some vapor-absent reactions are indicated by short lines extending from invariant points. The positions of thermal maxima are shown by dashed lines. See Introduction for explanation of abbreviations.

cal end-point on the univariant reaction Q + H_2O → L was placed at 1080°C and 9.7 kbar. Neither Stewart (1967) nor Warner (1973) accepted the existence of this critical end-point in their interpretations of experiments at 10 kbar, but Nakamura and Kushiro (1974) showed that SiO_2–H_2O is supercritical at 15 kbar.

Phase equilibrium studies and beta-track solubility measurements by Mysen and Seitz (1975) and Mysen *et al.* (1976) indicate that the solubility of CO_2 in silicate liquids remains low up to high pressures and that the solubility of CO_2 in silicate liquids decreases as the silica content of the liquid increases. These data indicate that the solubility of CO_2 in molten SiO_2 is much lower than that of H_2O, and we assume that the solubility of CO_2 in the supercritical fluid in SiO_2–H_2O above 9.7 kbar is negligible. Schematic phase relationships in the system SiO_2–H_2O–CO_2 have been illustrated for various pressures by Wyllie and Haas (1965), Boettcher and Wyllie (1969), and Eggler (1975). Similar diagrams are used in the following pages, but there are no univariant reactions for this system plotted in Figure 1.

MgO–H_2O–CO_2

This system was modeled in detail by Ellis and Wyllie (1979a) at pressures up to 100 kbar. Irving and Wyllie (1975) and Huang and Wyllie (1976) determined that the magnesite dissociation reaction MC → Pe + CO_2 is terminated by melting at an invariant point (Br,En,Fo,Q) in Figure 1 at 23 kbar and 1550°C. Ellis and Wyllie (1979a) postulated that brucite melts similarly at an invariant point (En,Q,Fo,MC), estimated to be near 57 kbar and 1310°C, and that the ternary reaction for dissociation of the assemblage magnesite plus brucite is terminated by melting at the invariant point (En,Q,Fo), estimated to be near 46 kbar and 1210°C. At pressures above this invariant point, brucite, magnesite, and vapor, buffered to high H_2O/CO_2, melt together in a eutectic reaction. The composition of the eutectic liquid on the vapor-absent join $Mg(OH)_2$–$MgCO_3$ was estimated by Ellis and Wyllie (1979a) to be 73 mole percent $Mg(OH)_2$ plus 27 mole percent $MgCO_3$.

There are divariant surfaces for dissociation and melting reactions occurring in the presence of H_2O–CO_2 vapor that connect the lines meeting at the three invariant points discussed above. Ellis and Wyllie (1979a) derived thermodynamic parameters from ln fugacity *vs.* $1/T$ diagrams and calculated the locations of contours of constant vapor phase composition on these surfaces. Their Figure 5 showed contours on surfaces for the reactions MC → Pe + CO_2 (with H_2O present) and MC + H_2O → Br + CO_2. Vapor in the presence of magnesite is buffered to high values of H_2O/CO_2 except for a narrow pressure interval just above the reaction MC → Pe + CO_2.

MgO–SiO_2–H_2O

Ellis and Wyllie (1979b) presented a model for hydration and melting reactions in this system up to 100 kbar. Subsolidus and melting relations were tied together into an internally consistent *P–T* net, reproduced in part in Figure 1. The solidus curves for forsterite plus vapor, forsterite plus periclase plus vapor, and forsterite plus enstatite plus vapor extend to lower temperatures with increasing pressure, and they are intersected by hydration curves bringing brucite to the liquidus at the invariant points (En,Q,Mc) and (Pe,Q,MC) at pressures near 50 and 90 kbar, respectively. The incongruent melting curve for enstatite, En + H_2O → Fo + L, terminates at the 90 kbar invariant point. At pressures above 90 kbar, forsterite cannot coexist with H_2O because it must react to produce brucite, and the assemblage enstatite plus vapor melts incongruently to produce brucite plus liquid.

MgO–SiO_2–CO_2

Wyllie and Huang (1976) combined experimental data available to 33 kbar in this system and estimated

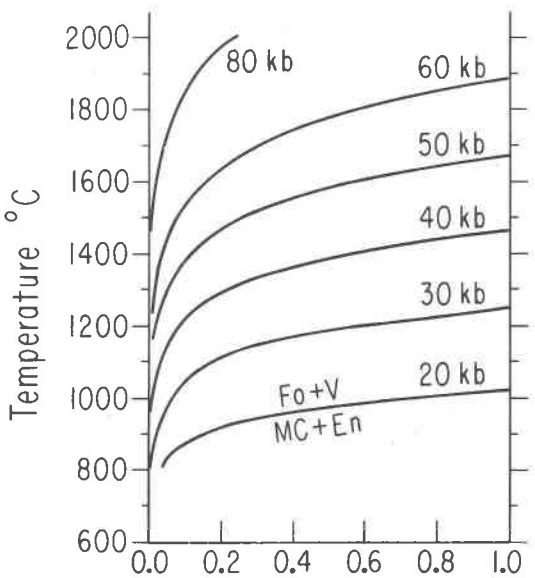

Fig. 2. Isobaric T–X_{CO_2} diagrams showing the position of the reaction MC + En → Fo + V at pressures of 20, 30, 40, 50, 60, and 80 kbar. Positions calculated using CO_2 fugacities predicted by the MRK equation and the thermodynamic data of Eggler *et al.* (1979).

the phase relationships to 70 kbar. Univariant reactions with vapor are reproduced in Figure 1, and the solidus reaction is extended to 100 kbar. With increasing pressure, there are three successive carbonation reactions which terminate on the solidus at the invariant points (Br,En,Q), (Pe,Br,Q), and (Pe,Br,Fo). The silicate mineral melting with magnesite and CO_2 along the solidus curve changes at each invariant point, from forsterite to enstatite to quartz, with increasing pressure.

The system MgO-SiO_2-H_2O-CO_2

General remarks

A network of binary, ternary, and quaternary univariant reactions is given in Figure 1 as a framework for the detailed discussions that follow. The details needed to supplement the *P–T* projection of Figure 1 are illustrated in a series of isobaric diagrams at successively higher pressures (Figs. 2, 4, 5, 6, and 8) and a series of *P–T* diagrams (Figs. 3, 7, 9, and 10), showing the changes that occur at invariant points. Particular attention is paid to the changes associated with assemblages including forsterite plus enstatite.

Isobaric equilibrium liquidus diagrams shown in Figure 4 are based on the ternary relationships reviewed above and quaternary relationships related to divariant surfaces similar to those illustrated in Figures 3B and 3C. The heavy lines in MgO–H_2O–CO_2 and MgO–SiO_2–CO_2 are the vapor-saturated liquidus field boundaries, which give the compositions of liquids coexisting with crystals and with H_2O–CO_2 or CO_2 vapor. The heavy lines in MgO–SiO_2–H_2O show the compositions of H_2O-saturated liquids merging continuously through a fluid phase into the H_2O-rich vapor phase coexisting with liquids on the other side of the miscibility gap. Field boundaries have been omitted from SiO_2–H_2O–CO_2 for clarity. The limiting phase boundary in this triangle is assumed to pass from the liquidus on SiO_2–CO_2 towards the corner

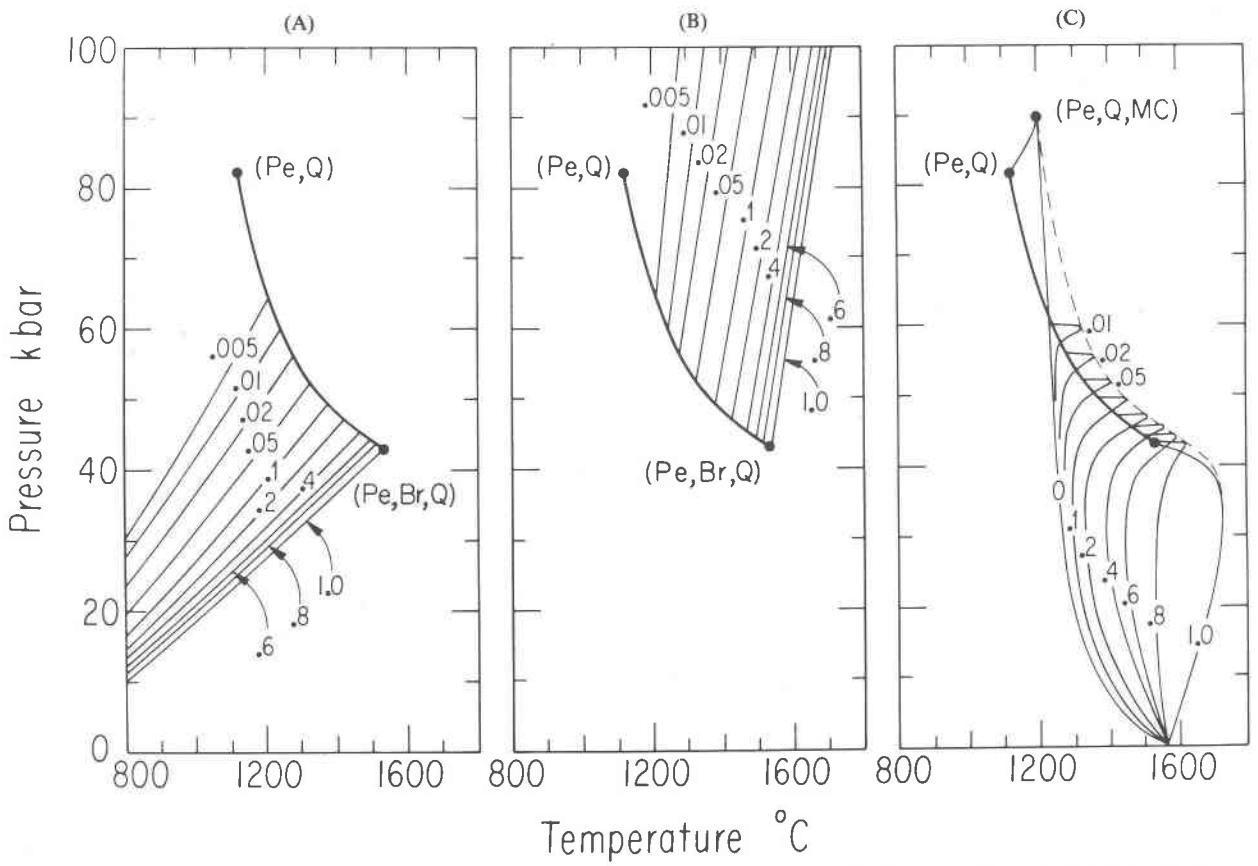

Fig. 3. Vapor-phase contours (mole fraction of CO_2) on three significant divariant surfaces in the system MgO–SiO_2–H_2O–CO_2. These three divariant surfaces meet along the heavy line, which is the buffered melting reaction MC + En + V → Fo + L. A shows contours on the surface for the reaction MC + En → Fo + V. B shows contours on the surface for MC + En + V → L. C shows contours on the surface for the reaction Fo + En + V → L. Note the presence of a thermal maximum (shown by a dashed line) in the contours for Fo + En + V → L.

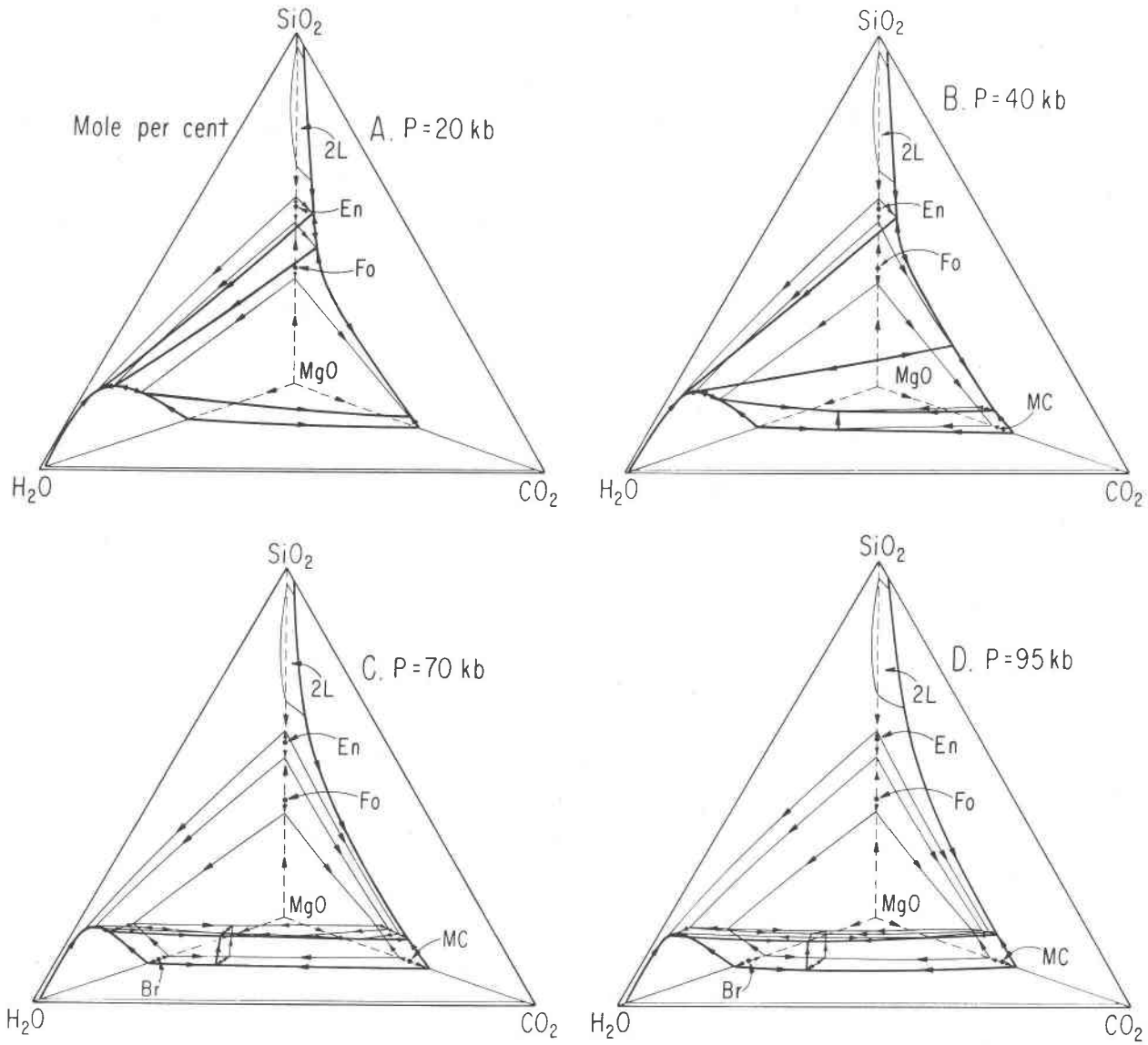

Fig. 4. Schematic isobaric liquidus diagrams for the studies $MgO–SiO_2–H_2O–CO_2$ at 20, 40, 70, and 95 kbar. Boundaries on the vapor-saturated surface are shown as heavy lines. These diagrams are derived from Fig. 1.

H_2O, with very little CO_2 being dissolved in the liquid and fluid phases of $SiO_2–H_2O$. There is a continuous vaporus boundary close to the join $H_2O–CO_2$, similar to that shown for $MgO–H_2O–CO_2$.

The quaternary vapor-saturated liquidus surface connects the heavy lines of the bounding ternary systems, merging through a small area for quaternary fluid near the H_2O end of $SiO_2–H_2O$, into the narrow vaporus surface situated close to $H_2O–CO_2$. The geometry of a similar surface in $CaO–SiO_2–H_2O–CO_2$ was illustrated by Boettcher and Wyllie (1969).

Isobaric invariant points for the system $MgO–SiO_2$ are marked on that join, and ternary field boundaries separating liquidus areas for the crystallization of periclase, forsterite, enstatite, and quartz extend from these points to the vapor-saturated field boundaries in $MgO–SiO_2–H_2O$ and $MgO–SiO_2–CO_2$. These areas extend into the quaternary system as volumes separated by surfaces which terminate as liquidus field boundaries on the vapor-saturated liquidus surface.

The field boundaries on the vapor-saturated liquidus surface are illustrated in Figure 5, where the vapor-saturated surface is projected from the MgO corner of the tetrahedron onto the face $SiO_2–H_2O–$

CO_2. The projections of these surfaces in Figure 5 show both the vapor-saturated liquidus field boundaries and the intervening primary phase fields. The immiscible fields (2L) shown in $MgO–SiO_2–H_2O$ and $MgO–SiO_2–CO_2$ have not been represented on the quaternary surfaces in Figures 4 and 5.

The schematic T-X_{CO_2} diagrams given in Figure 6 represent a series of isobaric slices through Figure 1. These diagrams are used to illustrate the details of the links between subsolidus and liquidus phase relationships indicated in Figures 1 and 3. Univariant lines are connected through the system by divariant surfaces. For example, the pair of binary reactions Fo + H_2O → L and Fo + CO_2 → L represent two ends of one divariant P–T–X surface for the ternary melting reaction Fo + V → L, which can be contoured in P–T projection by lines of constant vapor-phase composition.

Each quaternary vapor-saturated liquidus field boundary from Figures 4 and 5 is illustrated schematically in Figure 6 in terms of temperature and the composition of the coexisting vapor-phase composition. The arrows for falling temperature in Figures 4 and 5 are translated into slopes in Figure 6.

In addition, Figure 6 shows lines for the congruent melting of forsterite and enstatite in the presence of vapor, which are isobarically univariant by restriction (Ricci, 1951, p. 25). In Figures 4 and 5, these reactions are represented by temperature maxima (not marked) where the surfaces Fo–H_2O–CO_2 and En–H_2O–CO_2 intersect the vapor-saturated liquidus surface. The assemblage enstatite plus vapor melts congruently for CO_2-rich vapors, but incongruently for H_2O-rich vapors (Eggler, 1975). The change occurs at the singular point (Fig. 6) where the reaction En + V → L merges with the four-phase reaction including forsterite and where the field boundary in Figure 5A crosses the composition join enstatite–H_2O–CO_2.

Construction of these figures required considerable extrapolation from known data and repeated checking back and forth between Figures 4 and 6 and Figure 1, in order to maintain internal consistency. Although many pressures, temperatures, and compositions need to be determined precisely, we believe that the geometrical constraints are sufficient to ensure that the sequence of phase relationships illustrated provides an accurate representation of the melting and crystallization processes for phase assemblages involving forsterite and enstatite with H_2O–CO_2 vapor, magnesite, and brucite.

Subsolidus reactions in the system $MgO–SiO_2–H_2O–CO_2$

The ternary subsolidus reactions involving H_2O or CO_2 are univariant, and pairs of analogous reactions are connected through the quaternary system by

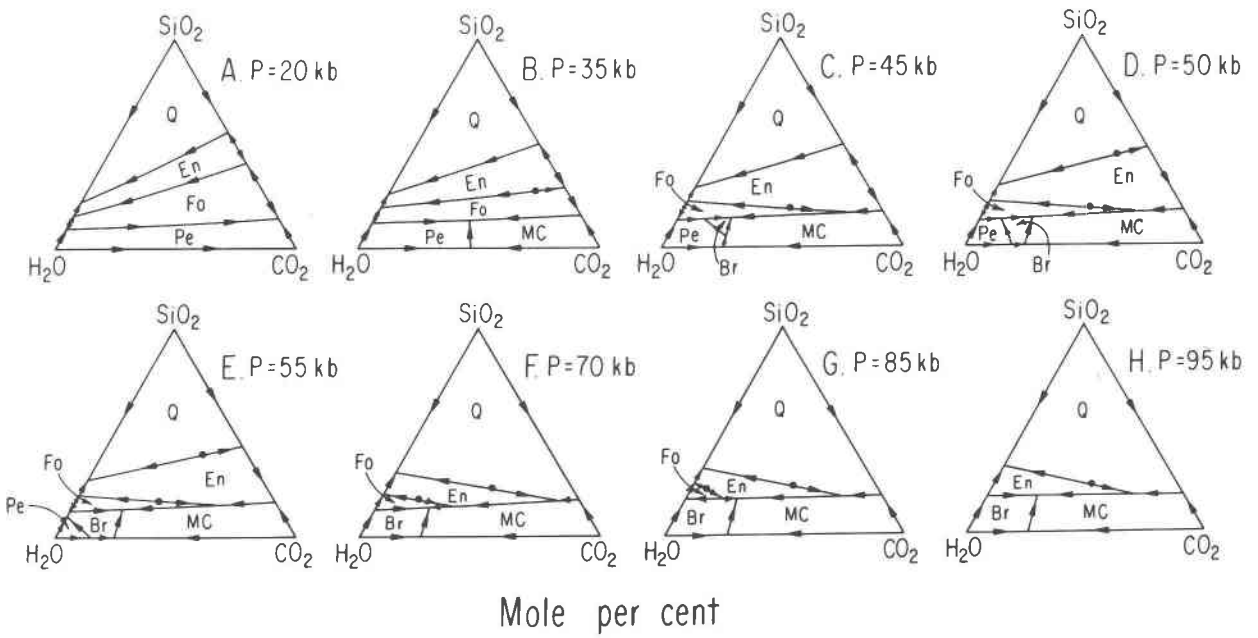

Fig. 5. Projections of vapor-saturated liquidus surfaces in the system $MgO–SiO_2–H_2O–CO_2$ at pressures of 20, 35, 45, 50, 55, 70, 85, and 95 kbar onto the plane $SiO_2–H_2O–CO_2$. Projected from the MgO corner of the $MgO–SiO_2–H_2O–CO_2$ tetrahedron. Two-liquid fields are not shown. The positions of thermal maxima are shown by dots.

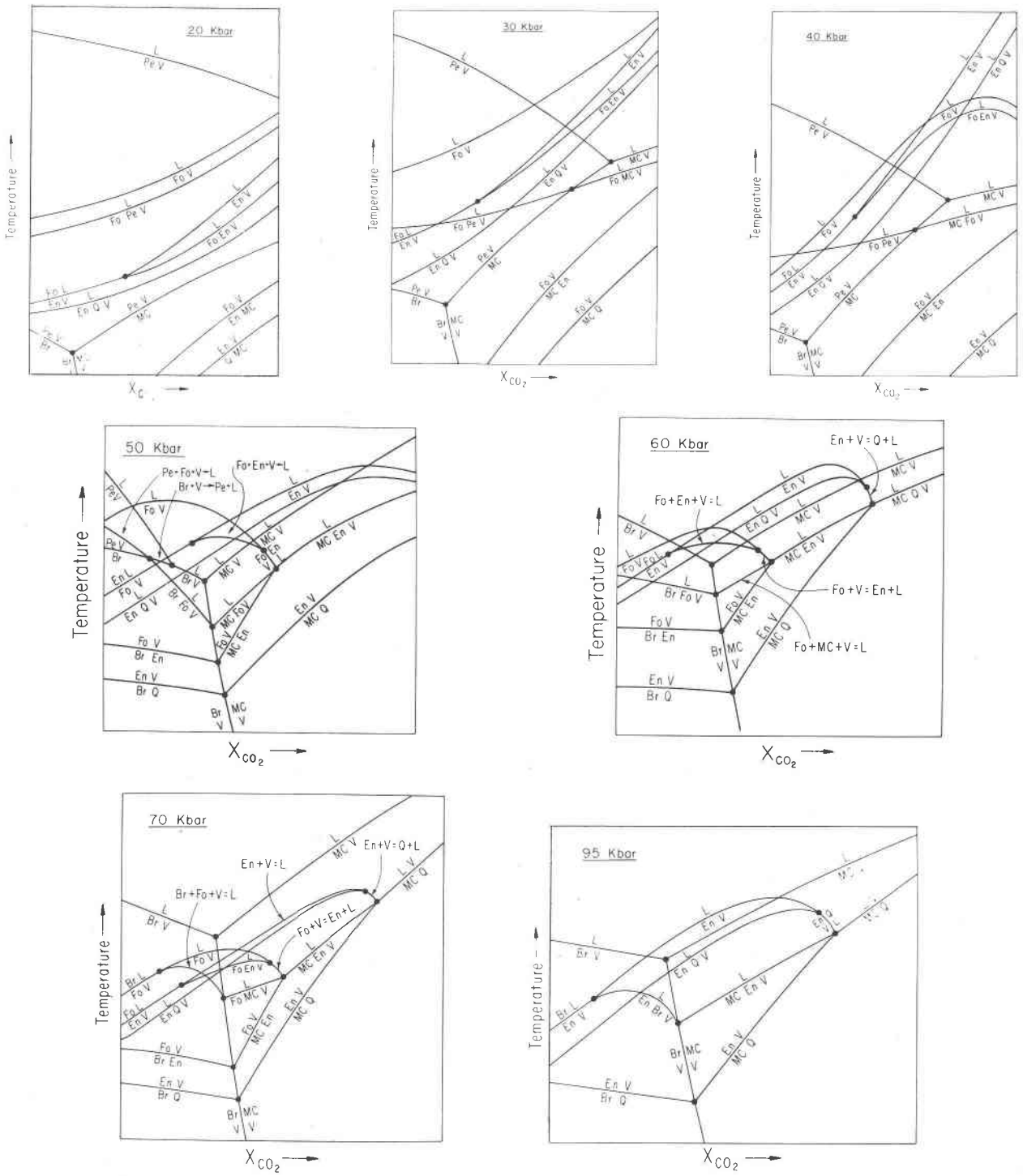

Fig. 6. Schematic isobaric T–X_{CO_2} diagrams showing the interrelation of subsolidus and melting reactions in the system MgO–SiO_2–H_2O–CO_2 at pressures of 20, 30, 40, 50, 60, 70, and 95 kbar.

divariant surfaces corresponding to these reactions occurring in the presence of H_2O–CO_2 mixtures. The points of lowest temperature on the surfaces define the univariant reaction for dissociation of a carbonate and hydrate together (in isobaric T–X_{CO_2} diagrams, these points occur at the intersection of two reaction lines).

There is one quaternary univariant subsolidus re-

action in Figure 1, Br + MC + En → Fo + V. Given the data of Eggler *et al.* (1979) plus the molar volume data of Robie and Waldbaum (1968), one may derive the reaction

$$\ln f_{CO_2} = -21337/RT + 0.1888(P - 1)/T + 41.05$$

This relationship may be used in conjunction with the fugacities predicted by the MRK equation (Holloway, 1976, 1977) to predict the quaternary T–X_{CO_2} relations shown in Figure 2.

The T–X_{CO_2} relations shown in Figure 2 and in Figure 3 of Ellis and Wyllie (1979a) may be used to position contours of constant vapor-phase composition for the assemblages containing forsterite plus enstatite, together with magnesite or brucite. The surface plotted by isobaric contours in Figure 2 is illustrated in Figure 3A by contours for constant vapor-phase composition. Its position in Figure 1 can be located by the positions of the invariant points (Pe,Br,Q) near 43 kbar and (Pe,Q,MC) near 90 kbar. The surface is terminated by melting along the quaternary univariant solidus curve for the reaction, MC + En + V → Fo + L, that connects these invariant points.

Note the strong buffering capacity of magnesite. If both magnesite and brucite are present, the fugacities of H_2O and CO_2 are controlled by the reaction MC + H_2O → Br + CO_2, and Figures 2 and 3A show that, for the quaternary reaction Br + MC + En → Fo + V extending below point (Pe,Q) in Figure 1, this control drives the vapor-phase composition to very high values of H_2O/CO_2. Forsterite and vapor cannot coexist at pressures greater than that of the quaternary subsolidus reaction.

Phase relationships from 1 bar to (Br,En,Q) at 23 kbar

The low-pressure phase relationships involving forsterite and enstatite in MgO–SiO_2–H_2O were reviewed by Ellis and Wyllie (1979b). At pressures above a few kbar, forsterite and enstatite both melt congruently, as shown in Figure 4A. Figures 4A and 5A show that they also melt congruently in the presence of CO_2, but that in the presence of H_2O forsterite melts congruently and enstatite melts incongruently. The vapor-saturated liquidus boundary between the fields giving the compositions of liquids generated from forsterite plus enstatite plus vapor is forsterite–enstatite-normative in the presence of CO_2 (with a small amount of dissolved CO_2) and enstatite–quartz-normative in the presence of H_2O (with a high percentage of dissolved H_2O). The position of the surface between the volumes for forsterite and enstatite in Figure 4A illustrates the contrasting effects of H_2O and CO_2 on the compositions of liquids developed from the assemblage forsterite plus enstatite. The change in liquid composition from forsterite-normative to quartz-normative occurs at the singular point shown in Figure 6A where the field boundary crosses the surface enstatite–vapor (V is very close to H_2O–CO_2) in Figure 4A. This point, if plotted on the solidus surface in Figure 3A, would trace a line trending from CO_2 at low pressures towards H_2O at higher pressures. We have little information on the position of this important line, except for the data of Eggler (1975) at 20 kbar and the results of Mysen and Boettcher (1975a,b) on near-solidus liquids from peridotite–H_2O–CO_2.

At low pressure, the solubilities of H_2O and CO_2 are much lower than those at 20 kbar in Figure 4A. The vapor-saturated liquidus surface is therefore further away from the edge H_2O–CO_2 and nearer to MgO–SiO_2. The liquidus and vaporus surfaces do not merge near the joint SiO_2–H_2O until the second critical end-point is reached in SiO_2–H_2O (see review above). Because there are no invariant points between 1 bar and 23 kbar in Figure 1, the relative arrangement of phase boundaries depicted at 20 kbar in Figures 4A, 5A, and 6A is maintained through the pressure interval, 1–20 kbar.

With increasing pressure the carbonation and hydration reactions shown in Figures 1 and 3A increase considerably in temperature, and the divariant surfaces therefore move upward through Figure 6A. Melting reactions with H_2O decrease in temperature with increasing pressure, whereas melting reactions with CO_2 first increase in temperature and then decrease, as shown in Figure 1. With increasing pressure in this range, the subsolidus reactions in Figure 6A move towards the melting reactions.

Phase relationship from (Br,En,Q) at 23 kbar to (Pe,Br,Q) at 42 kbar

Figure 1 shows that the changes occurring in this pressure interval are caused by the fact that magnesite becomes stable at and above the solidus. Details of the changes occurring in MgO–SiO_2–CO_2 were presented by Wyllie and Huang (1976). Magnesite appears first on the ternary CO_2-saturated liquidus at the eutectic between forsterite and periclase (Figs. 4A and 5A). With increasing pressure the ternary magnesite field expands to include magnesite and expands into the vapor-absent region. The quaternary magnesite liquidus volume expands into the quaternary system as a wedge, separating the periclase volume from vapor, as shown in Figures 4B and 5B.

Phase relationships involving magnesite corre-

spond to those illustrated in Figures 4B and 5B through most of this pressure interval, but additional changes occur in $MgO–SiO_2–CO_2$, as illustrated in Figures 1, 4B, and 6C. According to Wyllie and Huang (1976), the liquidus surface for enstatite expands at the expense of that for forsterite, an expansion consistent with the experimental results of Eggler (1974) on forsterite–enstatite–diopside–CO_2. This expansion has the effect of moving the forsterite–enstatite surface in the tetrahedron down towards magnesite, as shown in Figure 4B (compare with Fig. 4A). This surface meets the magnesite phase volume at the invariant point (Pe,Br,Q) and, at higher pressures, the forsterite volume does not reach the CO_2-saturated liquidus at all, as shown in Figures 5C and 5D. Associated with this migration of the liquid derived from forsterite plus enstatite plus CO_2 is a marked increase in CO_2 solubility (Fig. 4B), a marked decrease in reaction temperature (Fig. 1), and a change in the melting of forsterite plus CO_2 from congruent to incongruent (Fig. 4B).

At some pressure near 35 kbar a new and previously undescribed feature of the system $MgO–SiO_2–H_2O–CO_2$ appears, due to the abrupt lowering of melting temperatures by CO_2. This feature is a thermal maximum on the reaction Fo + En + V → L. Its postulated location is shown in Figures 1 and 3A as a dashed line which passes just above the invariant point (Pe,Br,Q) and terminates very close to the point (Pe,Q,MC). The location of the thermal maximum is shown in other ways in Figures 4, 5, and 6. The origin of this significant feature, unidentified in other related studies (Eggler, 1975, 1978; Mysen and Boettcher, 1975a,b), will be described in detail.

Wyllie and Huang's (1976) model of the system $MgO–SiO_2–CO_2$ shows that the forsterite–enstatite–vapor solidus has a positive P–T slope at pressures up to about 30 kbar. According to their model it then undergoes a rapid decrease in temperature and intersects an invariant point at roughly 1550°C and 43 kbar. In contrast, the forsterite–enstatite–vapor solidus in the system $MgO–SiO_2–H_2O$, as modeled by Ellis and Wyllie (1979b), has no thermal maximum. It has negative P–T slope until it terminates at high pressure.

The three reactions which meet in the system $MgO–SiO_2–CO_2$ to generate the invariant point (Pe,Br,Q) must all correspond to divariant surfaces in the system $MgO–SiO_2–H_2O–CO_2$. Those three surfaces meet along the quaternary univariant reaction MC + En + V → Fo + L. The positions of $H_2O–CO_2$ contours on the subsolidus reaction MC + En → Fo + V have been calculated from the data of Eggler *et al.* (1979) and are shown in Figure 3A. The place where each calculated contour on the MC + En → Fo + V surface meets the quaternary univariant reaction MC + En + V → Fo + L determines where contours on the other two surfaces, shown in Figures 3B and 3C, must meet that line. In the absence of any data, the contours shown on the MC–En–L–V surface in Figure 3B are simply assumed to be roughly parallel to the reaction MC + En + CO_2 → L.

Vapor composition contours on the divariant surface Fo + En + V → L are constrained by the above-cited models of the boundary ternary systems, the 20-kbar data of Eggler (1979) and the 20-kbar data of Mysen and Boettcher (1975a,b). Both studies indicate that at 20 kbar the solidus temperature increases roughly 20°C for each 10 percent increase in the mole fraction of CO_2 in the vapor phase. If one assumes that at least the contours for vapor with very low $H_2O–CO_2$ ratios are similar in shape to the contour for pure CO_2, the thermal maximum in the system $MgO–SiO_2–CO_2$ must extend into the quaternary system and disappear at some intermediate vapor composition.

We suggest that the thermal maximum continues to exist at pressures up to about 90 kbar and that it persists to quite H_2O-rich vapor compositions. In Figure 3C the thermal maximum (shown as the dashed line) begins at about 35 kbar and ends near the invariant point (Pe,Q,MC) at 90 kbar. The detailed phase relations near the points (Pe,Q) and (Pe,Q,MC) are shown in Figure 7B. Analysis of phase relations at these points by Schreinemakers' rules requires that both pressure and temperature maxima exist on the Br–Fo–En–L–V reaction. This thermal maximum terminates the one which originates in $MgO–SiO_2–CO_2$ near 35 kbar. The explanation given in later sections of the way in which phase relations change at high pressures gives the details of the disappearance of the thermal maximum.

Physically, the thermal maximum on the forsterite–enstatite–vapor solidus is a thermal ridge on the solidus surface, as shown in Figure 3C, where the solidus meets the liquidus at points corresponding to the temperature maxima on isobaric forsterite–enstatite–vapor liquidus field boundaries.

At low pressures the congruent melting of forsterite, Fo + V → L, is represented by the crest of a thermal ridge on the liquidus surface, extending continuously from H_2O to CO_2. At pressures approaching the stabilization of magnesite at the solidus, the lowering of liquidus temperatures by CO_2 depresses

the thermal ridge, causing it to shrink and migrate away from the CO_2 side, with the result that the crest of the ridge has a temperature maximum for some intermediate vapor composition, as shown in Figure 6C.

The field boundary for Fo + En + V → L is a simple valley on the vapor-saturated liquidus surface at low pressures (Figs. 4A and 5A), but with its migration towards $MgCO_3$ (Figs. 4B and 5B), it approaches the thermal ridge associated with the congruent melting of forsterite plus vapor. The crest of this ridge falls away towards the CO_2 side (Fig. 6C), and as the forsterite–enstatite–vapor field boundary approaches, it traverses the flank of the ridge obliquely, passing over a temperature maximum before it can fall off to the lower temperatures required by the migrating position of its CO_2-rich end. This produces the temperature maximum shown in Figure 6C. At somewhat higher pressure, at the singular point near 40 kbar in Figure 1, the field boundary reaches the forsterite–CO_2 joint as described by Wyllie and Huang (1976). At higher pressures the field boundary crosses the forsterite–vapor ridge on its low-temperature CO_2 side and extends down towards the liquidus field for primary magnesite (see Figs. 5A, B, C, and D). The temperature maximum on the field boundary does not coincide precisely with the forsterite–vapor ridge crest, but is situated at a point within the volume forsterite–enstatite–vapor (as required by chemographic relationships), which is the highest point crossed as the field boundary traverses the flank of the forsterite–vapor ridge before crossing the ridge crest itself—the crest being at lower temperatures at points closer to the CO_2 side.

With increasing pressure, the forsterite–vapor ridge contracts further away from the CO_2 side, and the forsterite–enstatite field boundary moves progressively down towards $MgCO_3$. The vapor present at the temperature maximum consequently becomes richer in H_2O (Fig. 5) as does the coexisting vapor, as shown in Figures 3C and 6.

At pressures up to at least 20 kbar, H_2O/CO_2 is higher in liquid than in vapor for melting reactions involving forsterite plus enstatite (Eggler, 1975; Mysen and Boettcher, 1975a,b). At the temperature maximum on the field boundary, the chemographic relationships require that H_2O/CO_2 is the same in coexisting liquid and vapor; the dashed line in Figure 3C is the locus for this equality. On the carbonate side of the temperature maximum, therefore, H_2O/CO_2 is higher in vapor than in liquid. This is consistent with phase relationships in the system MgO–CO_2–H_2O (Ellis and Wyllie, 1979a). This condition exists for the portion of the surface in Figure 3C between the dashed line and the solid line for the buffered melting of partly carbonated forsterite–enstatite assemblage.

Phase relationships from (Pe,Br,Q) at 42 kbar to (En,Q,Fo,MC) at 58 kbar

In the pressure interval from 42 to 58 kbar, changes in melting relationships are due to two factors, as shown in Figure 1. Brucite becomes stable in

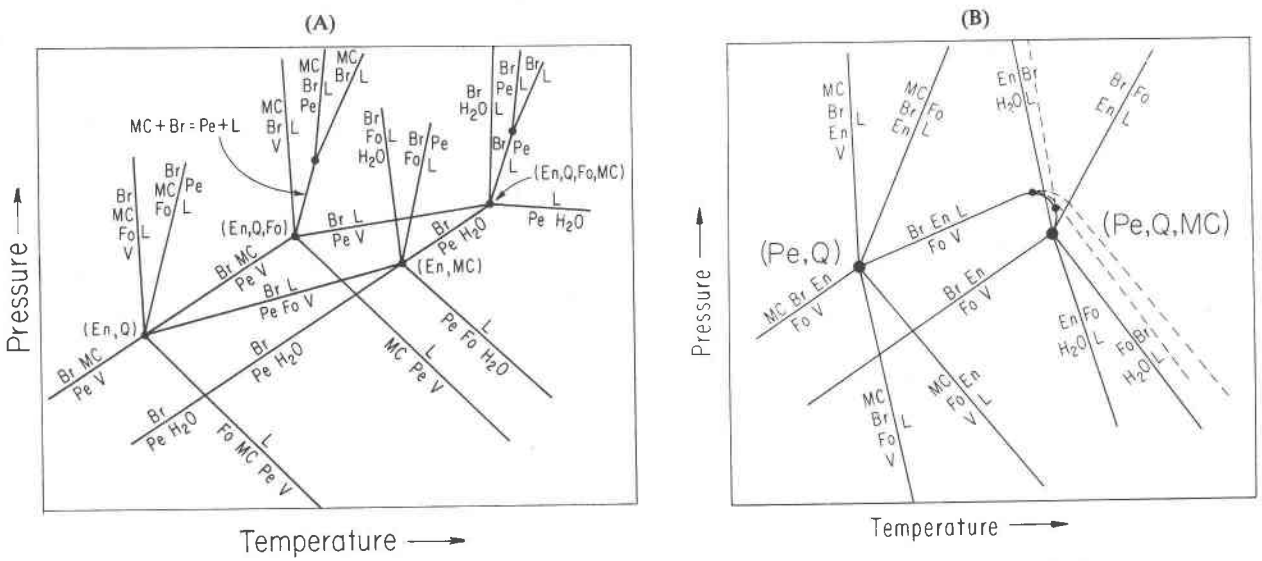

Fig. 7. Details of the topology of related groups of invariant points. Both vapor-present and vapor-absent reactions are shown. A shows invariant points near 50 kbar. B shows invariant points near 85 kbar. Not to scale.

the presence of vapor-saturated liquids, and as pressure increases the assemblage stable at the CO_2-saturated solidus changes from forsterite plus magnesite plus CO_2 to enstatite plus magnesite plus CO_2 to quartz plus magnesite plus CO_2.

Brucite first becomes stable in the presence of liquid at 44 kbar at the invariant point (En,Q) as shown schematically in Figure 7A, where a eutectic between forsterite, magnesite, brucite, and vapor replaces the eutectic stable at lower pressures between forsterite, magnesite, periclase, and vapor. Figure 5C illustrates how a crystallization volume for brucite has appeared and begun to cut off the periclase crystallization volume from the vapor-saturated liquidus. At 45 kbar the reaction MC + En → Fo + V has intersected the solidus, and the enstatite volume has begun to cut the forsterite volume off from coexisting with vapor. The thermal maximum on the reaction Fo + En + V → L moves to more H_2O-rich compositions for the same reason. The movement of the thermal maximum to more H_2O-rich compositions also shows in Figure 5C, D, and E, as well as the fact that the enstatite volume is cutting off the forsterite area on the vapor-saturated liquidus with increasing pressure.

At the invariant point (En,Q,Fo) shown in Figures 1 and 7A, brucite becomes stable in the system MgO–H_2O–CO_2. Schematic phase relations at 50 kbar are shown in Figures 5D and 6D. Figure 5D shows that, due to the expansion of the brucite crystallization volume, the peritectic reaction between periclase, magnesite, and vapor has been replaced by two new peritectics: between periclase, brucite, and vapor and between brucite, magnesite, and vapor. This change is reflected in the schematic T–X_{CO_2} section, Figure 6D, by the reactions Fo + Pe + V → L and Pe + V → L being replaced at isobaric invariant points by the reactions Fo + Br + V → L and Pe + V → Br + L. Figure 5E at 55 kbar illustrates how the periclase area on the vapor-saturated liquidus continues to contract as pressure increases until it is covered completely by brucite at the invariant point (En,Q,Fo,MC).

Phase relationships from (En,Q,Fo,MC) at 58 kbar to (Pe,Q) at 80 kbar

The invariant points (En,Q,Fo,MC) and (Pe, Br,Fo) lie at nearly the same pressure, about 58 kbar. Above that pressure periclase is not stable with vapor-saturated liquids, and quartz is the solidus silicate in the presence of pure CO_2. A T–X_{CO_2} diagram at 60 kbar, Figure 6E, shows that a second thermal maximum must be present at the reaction En + Q + V → L. This develops because that melting reaction crosses the enstatite–vapor thermal ridge at pressures above 40 kbar in the same way that the reaction Fo + En + V → L crosses the forsterite–vapor ridge at pressures above 35 kbar.

Ellis and Wyllie (1979b) demonstrated that the hydrous melting of forsterite must become incongruent between 50 and 90 kbar and arbitrarily placed that singular point at about 65 kbar. At pressures above that singular point, the reactions Fo + V → L and Br + Fo + V → L are stable only in the presence of mixed H_2O–CO_2 vapor. Figures 4C, 5F, and 6F show phase relations at pressures above the singular point at 65 kbar.

Comparison of the isobaric liquidus diagrams for 50 and 70 kbar (Figs. 4B and 4C, respectively) shows that by 70 kbar the crystallization volumes for quartz and enstatite have expanded to greater volatile and lower SiO_2 contents and that near the CO_2 corner of the tetrahedron they have begun to move away from the vapor-saturated liquidus surface across the top of the brucite–magnesite "prism."

The vapor-saturated liquidus surface shown in Figure 5F demonstrates more simply how much the crystallization volume of quartz has expanded relative to forsterite and enstatite. Comparison of Figure 6E and 6F shows that the range of X_{CO_2} over which forsterite melts congruently steadily decreases with increasing pressure.

Phase relationships from (Pe,Q) at 80 kbar to (Pe,MC,Q) at 90+ kbar

The topology of invariant points in the pressure range from 80 to 90+ kbar is shown in Figure 1 and in enlarged and detailed form in Figure 7B. At pressures greater than 80 kbar, forsterite may no longer coexist with vapor rich enough in CO_2 to stabilize magnesite. Figure 8A shows the water-rich part of the T–X_{CO_2} diagram at 85 kbar. The subsolidus reaction Br + En → Fo + V meets the solidus at the peritectic reaction between brucite, enstatite, forsterite, and vapor which is shown in Figure 8B. The small forsterite area on the vapor-saturated liquidus still stretches across both the forsterite–vapor and enstatite–vapor joins.

At the point (Pe,Q,MC) at 90 kbar, forsterite becomes unstable in the presence of pure H_2O, though for a narrow interval at slightly higher pressures it is stable with mixed H_2O–CO_2 vapor. At the point (Pe,Q,MC), the reactions En + Br → Fo + V, En + V → Fo + L, and Fo + V → Br + L meet at the H_2O

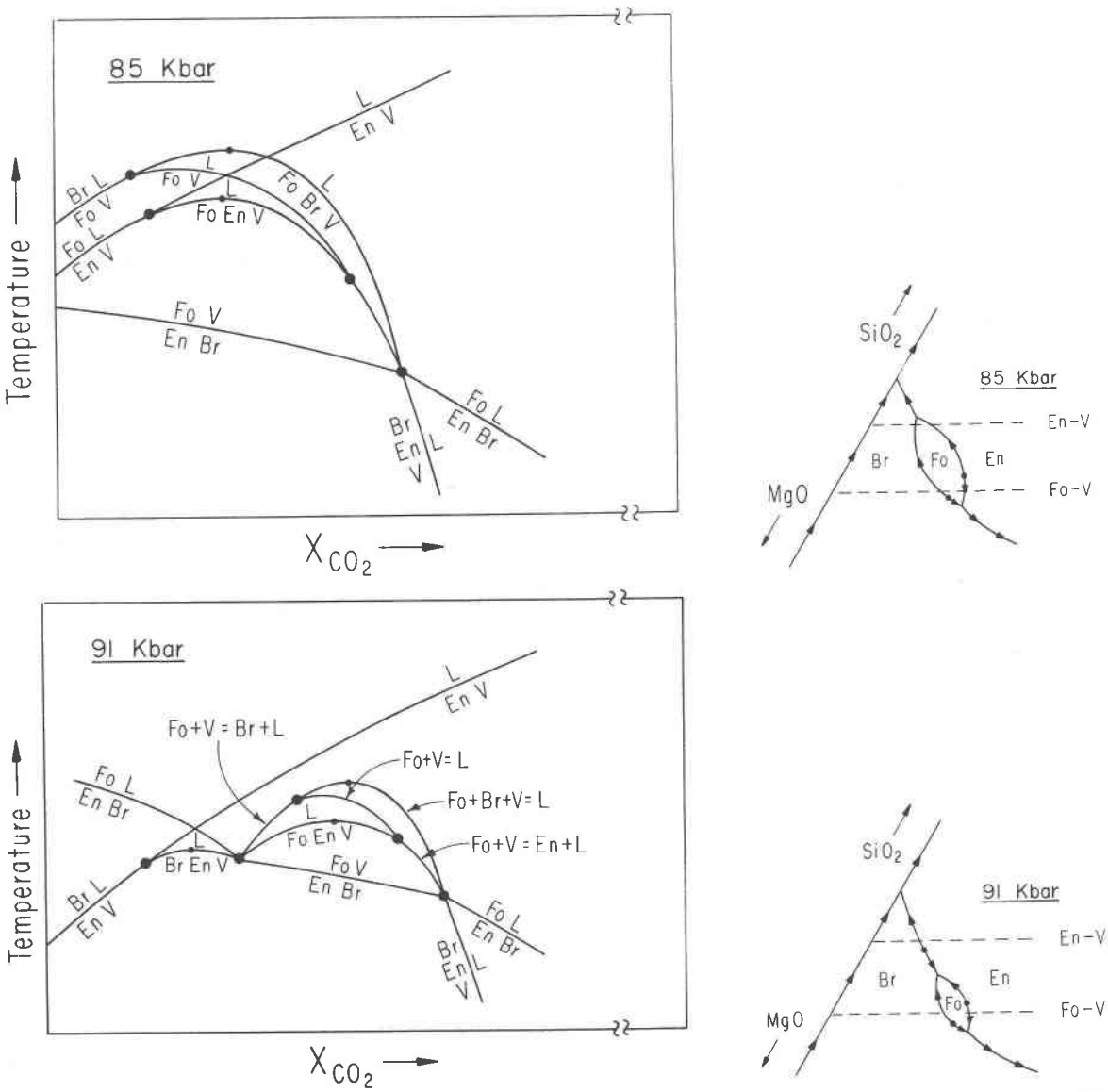

Fig. 8. The H_2O-rich portions of interest in T–X_{CO_2} and isobaric liquidus diagrams derived from Figure 7B at pressures of 85 and 91 kbar. Compare to Figures 4D, 5G, 5H, and 6G.

sideline of the T–X_{CO_2} diagram. As pressure increases, this peritectic reaction migrates toward more CO_2-rich vapor compositions, generating the topologies seen in Figures 8C and 8D at ~91 kbar.

When in Figure 8D the brucite–enstatite boundary migrates across the enstatite–vapor join, several things happen. The melting reaction immediately becomes congruent, a thermal maximum on the field boundary is soon created, and the boundary then terminates at a eutectic between forsterite, brucite, enstatite, and vapor. The field of forsterite on the vapor-saturated liquidus has been reduced to a tiny patch.

The T–X_{CO_2} topology at ~91 kbar is given in Figure 8C and shows that in a limited pressure interval temperature maxima exist on three melting reactions. The subsolidus reaction En + Br → Fo + V is terminated at both ends by invariant points involving the reactions En + Br → Fo + L and Br + En + V → L. Note, however, that one invariant point is a peritectic and the other is a eutectic. The fields for all assemblages and reactions containing forsterite plus vapor

are gradually narrowed as those two invariant points converge with increasing pressure. This corresponds to the convergence of the eutectic and peritectic at the ends of the forsterite field shown in Figure 8D. When the two invariant points meet with increasing pressure, the assemblage forsterite plus vapor is eliminated from the T–X_{CO_2} diagrams, and the forsterite area on the vapor-saturated liquidus disappears along with its two thermal maxima.

Phase relationships at pressures >95 kbar

At pressures greater than the invariant points (Pe,Q) and (Pe,Q,MC), phase relationships are considerably simpler. Schematic phase relationships at 95 kbar are shown in Figures 1, 4D, 5H, 6G, and 7B. Figure 7B shows that forsterite and vapor are never stable together at very high pressures. Enstatite takes the place of forsterite in vapor-present melting reactions, and forsterite is found only in vapor-absent assemblages. This is also illustrated in the 95-kbar isobaric liquidus diagrams, Figures 4D and 5H, which show that the volumes of forsterite and vapor do not meet at any point.

Figure 6G schematically shows the vapor-present subsolidus and melting relations at 95 kbar. Thermal maxima still exist in two reactions: En + Br + V → L and En + Q + V → L. Eutectics exist between brucite, magnesite, enstatite, and vapor and between brucite, magnesite, and vapor.

Estimates of liquid compositions

The compositions of liquids present at the solidus for bulk compositions of forsterite plus enstatite plus a small proportion of volatiles may be estimated from experimental evidence at low pressures in combination with isobaric liquidus diagrams, such as Figures 4A, B, C, and D. Estimates have been made at pressures of 20, 50, and 90 kbar for a bulk composition containing H_2O and CO_2 in a 3:1 mole ratio. The estimates are given in Table 1.

The experiments of Eggler (1975) demonstrate that at 20 kbar H_2O is partitioned toward the liquid phase. The experiments shown in his Figure 2 indicate that at 1450°C the $H_2O/(H_2O + CO_2)$ mole ratio in liquid coexisting with enstatite is about 0.77, while the vapor phase has an $H_2O/(H_2O + CO_2)$ mole ratio of 0.38. The results of Mysen and Boettcher (1975a,b) on the solidus in peridotite–H_2O–CO_2 are adopted for the slope of the divariant forsterite–enstatite–liquid–vapor melting surface: about 20°C per 0.1 increase in X_{CO_2} of the vapor. These two pieces of information may be used in combination to estimate that the liquid coexisting with forsterite plus enstatite plus vapor, whose $X_{CO_2} = 0.25$ at 20 kbar and about 1380°C, has an $H_2O/(H_2O + CO_2)$ mole ratio of 0.08. Given this estimate, one may calculate geometrically from the isobaric liquidus diagram, Figure 4A, the first liquid composition given in Table 1. This composition is SiO_2-saturated, in agreement with the conclusions of Eggler (1975) and Mysen and Boettcher (1975a,b). The high water content is due to the fact that the measured H_2O solubility in forsterite at 20 kbar is 65 mole percent (Hodges, 1973).

Table 1. Geometrically estimated compositions of first liquids coexisting with forsterite plus enstatite in a bulk composition with an H_2O/CO_2 ratio of 3/1

	MOLE PERCENT				WEIGHT PERCENT			
Pressure	MgO	SiO_2	H_2O	CO_2	MgO	SiO_2	H_2O	CO_2
20 kbar	12	17	70	1	18	37	45	0
50 kbar	34	10	31	25	38	17	15	30
90 kbar	32	18	39	11	36	31	19	14

The estimate at 50 kbar is less constrained. The subsolidus reaction MC + En → Fo + V buffers the vapor phase to an X_{CO_2} of 0.11 where its reaction intersects the buffered melting reaction at about 1400°C and 50 kbar. In order to estimate the liquid composition, we assumed that the slope of the melting reaction MC + Fo → L is similar to that of the reaction MC → L in the system $Mg(OH)_2$–$MgCO_3$. Using the P–T net given in Figure 2, one may then estimate that the $H_2O/(H_2O + CO_2)$ mole ratio of the liquid at 1400°C is roughly 0.4. This may be regarded as the maximum for the H_2O content of the liquid, because the slope of the vapor-present melting reaction would be expected to be shallower than that of the vapor-absent melting reaction. The estimated liquid composition given in Table 1 is therefore the most SiO_2-rich estimate possible. Even so, it is very low in SiO_2 and has large amounts of both H_2O and CO_2.

In the estimate of composition made at 90 kbar, the position of the $Mg(OH)_2$–$MgCO_3$ eutectic, calculated by Ellis and Wyllie (1979a), fixes the $H_2O/(H_2O + CO_2)$ mole ratio of the vapor-absent melt at 0.27. From that, geometric estimation of the liquid composition is straightforward. The composition of the liquid formed at high pressure has an intermediate SiO_2/MgO ratio. It has normative forsterite and enstatite and is high in volatiles. The quaternary eutectic between magnesite, enstatite, brucite, and forsterite would be expected to move farther from the vapor-saturated surface as pressure increases. There-

fore, liquids formed at higher pressures should be slightly higher in MgO and lower in volatiles.

The estimated compositions of first liquids change rapidly near 50 kbar, where the subsolidus reaction MC + En → Fo + V intersects the solidus. A bulk composition that produces an H_2O-rich, SiO_2-saturated first liquid at lower pressures produces a CO_2-rich, low SiO_2 liquid near 50 kbar and a liquid of intermediate SiO_2 content with $H_2O > CO_2$ at higher pressures. These same trends of melt composition

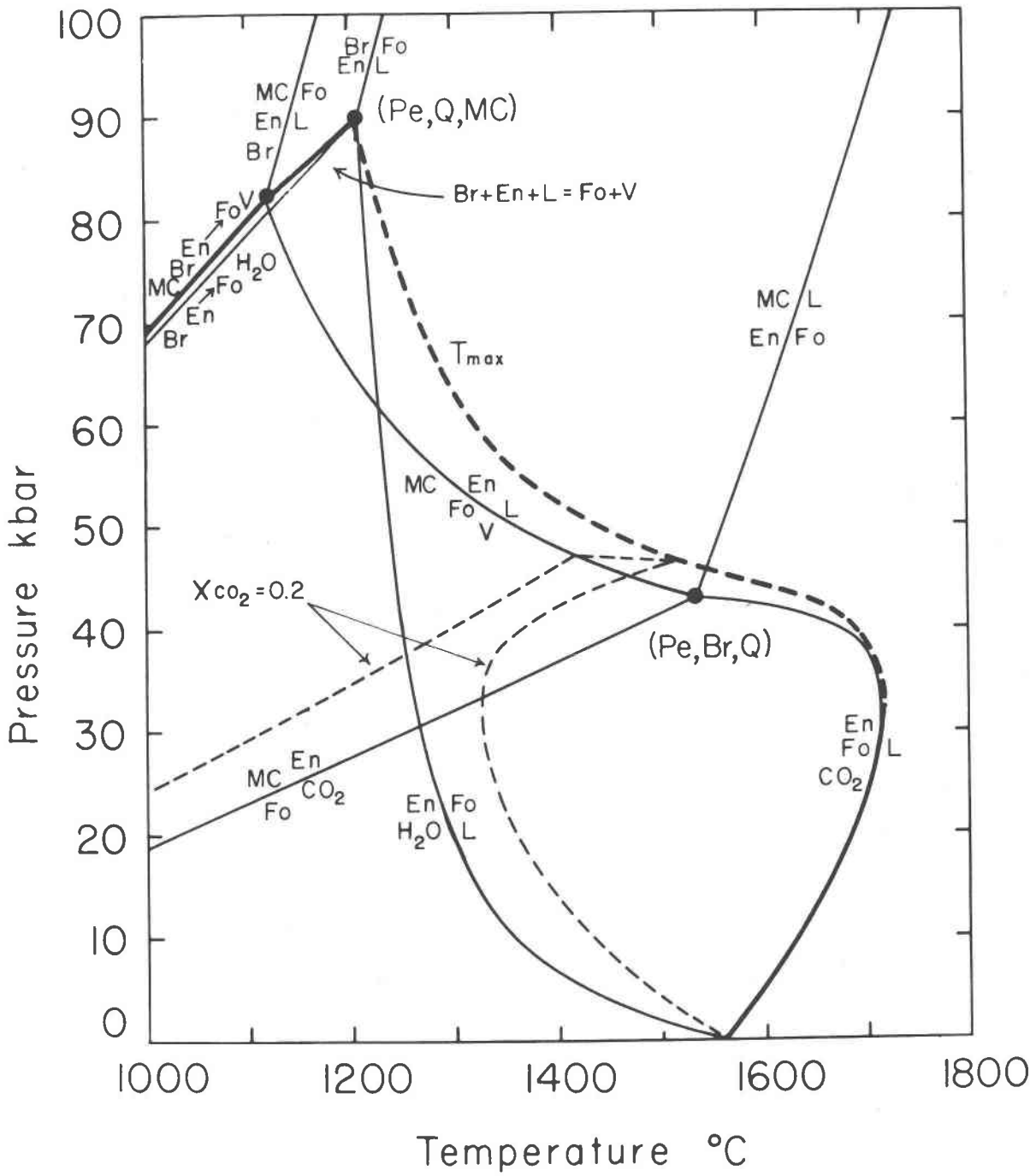

Fig. 9. Partial P–T net for the system MgO–SiO_2–H_2O–CO_2. Only reactions involving the assemblage forsterite plus enstatite are shown. Forsterite and vapor may coexist only in the P–T region enclosed by the heavy lines. The heavy dashed line shows the position of the thermal maximum on the reaction Fo + En + V → L.

with increasing pressure should also occur in the mantle system, although certainly at lower pressure, as shown by Wyllie (1978) and Eggler (1978). The data for the system $MgO–SiO_2–H_2O–CO_2$ suggest that the liquid present in the upper part of the low-velocity zone is likely to be carbonatitic, whereas that in the lower part of the low-velocity zone should be kimberlitic in composition.

Discussion

The model proposed for the system $MgO–SiO_2–H_2O–CO_2$ gives an internally consistent explanation for both the experimentally observed subsolidus and melting reactions and the effects of mixed $H_2O–CO_2$ vapor on those reactions. The model allows prediction of phase relations at pressures up to 100 kbar, where detailed experimental work is not presently feasible. The system contains the assemblage forsterite plus enstatite; H_2O and CO_2; a hydrate, brucite; and a carbonate, magnesite. Although many compositions in the system $MgO–SiO_2–H_2O–CO_2$ are far removed from those of the upper mantle, the relationships among these phases indicate the general features of phase relationships between those types of compounds in the upper mantle.

Figures 9 and 10 show respectively the reactions and mineral assemblages containing both forsterite and enstatite as a function of temperature and pressure. They show clearly that the stability of forsterite plus vapor is restricted by reactions producing enstatite plus a hydrate, a carbonate, or both. Forsterite and vapor do not coexist at pressures greater than that of the invariant point (Pe,MC,Q) at about 90 kbar. The low P–T field within which forsterite and vapor coexist is circumscribed by a heavy line in Figure 9. The processes of vapor-present melting and mantle metasomatism can occur only at pressures and temperatures within this field and are therefore restricted to depths less than 270 km. In the more complex system $CaO–MgO–Al_2O_3–SiO_2–H_2O–CO_2$, the region of vapor-present forsterite reactions may be restricted to a smaller pressure interval, due to the fact that reactions involving diopside occur at lower pressures than analogous reactions involving enstatite.

The model developed for the system $MgO–SiO_2–H_2O–CO_2$ requires that, in successively higher pressure ranges, three different types of melting processes characterize the melting of forsterite plus enstatite in the presence of $H_2O–CO_2$ vapor.

(1) At low pressures, the melting reaction is either enstatite + vapor → forsterite + liquid at low X_{CO_2} or

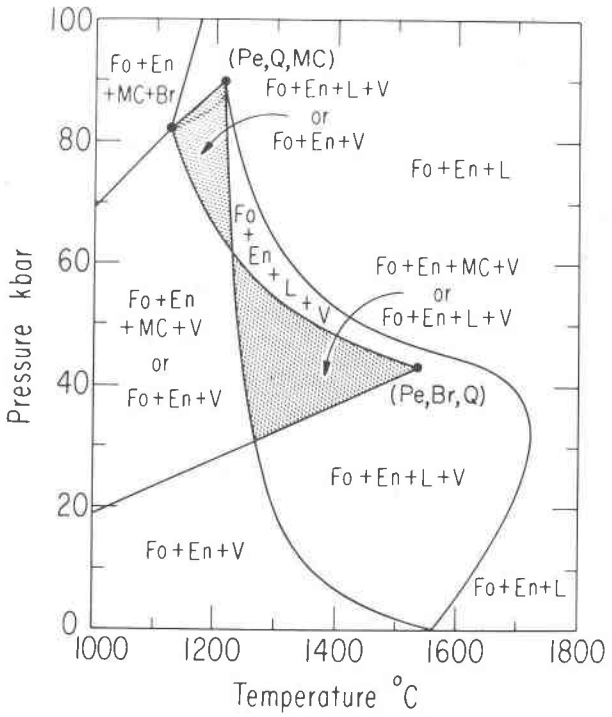

Fig. 10. Assemblages involving forsterite plus enstatite as a function of pressure and temperature. Note that forsterite and vapor do not coexist at high pressures or high temperatures.

forsterite + enstatite + vapor → liquid at high X_{CO_2}. The composition of the liquids produced varies from quartz-normative in the presence of H_2O to forsterite-normative in the presence of CO_2. This agrees with the conclusions of Eggler (1975) and Mysen and Boettcher (1975a,b). At 20 kbar H_2O is partitioned toward silicate liquids, and CO_2 is partitioned toward the coexisting vapor.

(2) At pressures between 42 and 80 kbar, the important melting reaction is Fo + MC + V → En + L. The composition of the vapor phase taking part in this reaction is buffered by the subsolidus reaction En + MC → Fo + V. At temperatures above the solidus for the assemblage forsterite plus enstatite, a thermal maximum exists on the reaction forsterite + enstatite + vapor → liquid. The X_{CO_2} of the vapor at this thermal maximum rapidly becomes smaller as pressure increases.

(3) At pressures above 90 kbar, forsterite plus enstatite melts at a quaternary eutectic with brucite and magnesite with no vapor present. H_2O/CO_2 mole ratio of the liquid is fixed at about 3/1 by the eutectic between $Mg(OH)_2$ and $MgCO_3$.

The composition of the first liquid formed in bulk compositions of forsterite plus enstatite and a small amount of volatiles with 3/1 H_2O/CO_2 ratio changes

from quartz-normative to periclase–forsterite-normative to enstatite–forsterite-normative as pressure increases.

These three kinds of melting reactions must also occur in peridotite, where H_2O and CO_2 are present as vapor or are stored in amphibole, phlogopite, and carbonate. The distribution of H_2O and CO_2 among liquid, crystals, and vapor in the simple system $MgO–SiO_2–H_2O–SiO_2$ provides a guide for interpretation of the phase relationships in the complex peridotite–H_2O–CO_2 system (Wyllie, 1978).

Two sorts of incongruent melting of silicate minerals occur in the system $MgO–SiO_2–H_2O–CO_2$ at high pressure. In the presence of H_2O–rich vapor, melts richer in SiO_2 than the mineral are produced; however, in the presence of CO_2-rich vapor, the silicates melt incongruently to give a liquid poorer in SiO_2 than the mineral. The $T–X_{CO_2}$ diagrams in Figure 6 show that the incongruent melting reactions originate at invariant points where related congruent melting reactions terminate. For example, in Figure 6F the incongruent melting reactions En + V → Fo + L and Fo + V → En + L both originate at invariant points where the congruent melting reaction Fo + En + V → L terminates. Figures 1 and 6 show that as pressure increases the X_{CO_2} range over which the melting of forsterite plus enstatite is congruent decreases until congruent melting disappears at the pressure at which the thermal maximum disappears. The $T–X_{CO_2}$ diagrams in Figure 6 also show that all reactions with the thermal maxima terminate at invariant points involving incongruent melting reactions.

The existence of a thermal maximum on the reaction Fo + En + V → L has important consequences. The thermal maximum is required at pressures above 35 kbar, as demonstrated earlier. It always occurs at a vapor composition richer in H_2O than the vapor at the intersection of the reactions Fo + En + V → L and MC + En → Fo + V. This requires the thermal maximum to move to H_2O-rich vapor compositions within a small pressure interval after it appears. The size of the maximum is postulated to decrease as it moves to more water-rich compositions. The thermal maximum occurs where the H_2O/CO_2 ratios in the liquid and vapor are equal. Such a thermal maximum presumably exists also in the complex mantle system, as discussed by Wyllie (1978).

Thermal maxima could be responsible for the rapid eruption of kimberlites from the upper mantle. The fact that melts present in the earth's upper mantle at pressures greater than 25 kbar are kimberlitic or carbonatitic has been postulated by Wyllie (1978) on the basis of experimental evidence. If a parcel of mantle whose temperature was just above its solidus were rising and encountered a thermal maximum on its solidus, all melt would crystallize and dissolved gases would be exsolved. If the parcel of mantle continued to rise and also retained its volatiles, it would recross its solidus and would partially melt. However, the composition of the partial melt would be different. The data of Bultitude and Green (1971) and of Brey and Green (1975) indicate that the liquid formed by remelting would be an olivine melilitite rather than a carbonatite.

A more likely series of events would have a fracture initiated due to the increased volume of the exsolved gases when the thermal maximum is first crossed. Once initiated, such a fracture could propagate very rapidly (Anderson, 1977). The fact that carbonatitic and kimberlitic liquids are extremely fluid would allow them to migrate easily to the fracture to continue its propagation. The rapid influx of melt and upward propagation of a fracture would make possible quick transportation of xenoliths and magma to a shallow depth, where wholesale exsolution of volatiles from the magma could initiate the violent surface eruption characteristics of kimberlites.

Acknowledgments

This research was supported by NSF grant EAR 76-20410 (Earth Sciences Section).

References

Anderson, O. L. (1977) Stress corrosion crack propagation as a possible mechanism for kimberlite pipe formation. *Extended Abstracts, Second International Kimberlite Conference, Santa Fe, New Mexico.*

Boettcher, A. L. and P. J. Wyllie (1969) The system $CaO–SiO_2–CO_2–H_2O$—III. Second critical end-point on the melting curve. *Geochim. Cosmochim. Acta, 33,* 611–632.

Brey, G. and D. H. Green (1975) The role of CO_2 in the genesis of olivine melilitite. *Contrib. Mineral. Petrol., 49,* 93–103.

——— and ——— (1976) Solubility of CO_2 in olivine melilitite at high pressures and role of CO_2 in the earth's upper mantle. *Contrib. Mineral. Petrol., 55,* 217–230.

Bultitude, R. J. and D. H. Green (1971) Experimental study of crystal–liquid relationships at high pressures in olivine nephelinite and basanite compositions. *J. Petrol., 12,* 121–147.

Eggler, D. H. (1974) Effect of CO_2 on the melting of peridotite. *Carnegie Inst. Wash. Year Book, 73,* 215–224.

——— (1975) CO_2 as a volatile component of the mantle: the system $Mg_2SiO_4–SiO_2–H_2O–CO_2$. *Phys. Chem. Earth, 9,* 869–881.

——— (1976a) Does CO_2 cause partial melting in the low-velocity layer of the mantle? *Geology, 4,* 69–72.

——— (1976b) Composition of the partial melt of carbonated peridotite in the system $CaO–MgO–SiO_2–CO_2$. *Carnegie Inst. Wash. Year Book, 75,* 623–626.

——— (1978) The effect of CO_2 upon partial melting of peridotite in the system Na_2O–CaO–Al_2O_3–MgO–SiO_2–CO_2 to 35 kbar, with an analysis of melting in a peridotite–H_2O–CO_2 system. *Am. J. Sci., 278,* 305–343.

———, I. Kushiro and J. R. Holloway (1979) Free energies of decarbonation reactions at mantle pressures: I. Stability of the assemblage forsterite–enstatite–magnesite in the system MgO–SiO_2–CO_2–H_2O to 60 kbar. *Am. Mineral., 64,* 288–293.

Ellis, D. E. and P. J. Wyllie (1979a) Carbonation, hydration, and melting relations in the system MgO–H_2O–CO_2 at pressures up to 100 kbar. *Am. Mineral., 64,* 32–40.

——— and ——— (1979b) Hydration and melting reactions in the system MgO–SiO_2–H_2O at pressures up to 100 kbar. *Am. Mineral., 64,* 41–49.

Green, D. H. (1976) Experimental testing of "equilibrium" partial melting of peridotite under water-saturated high-pressure conditions. *Can. Mineral., 14,* 255–268.

Greenwood, H. J. (1962) Metamorphic reactions involving two volatile components. *Carnegie Inst. Wash. Year Book, 61,* 82–85.

——— (1967) Mineral equilibria in the system MgO–SiO_2–H_2O–CO_2. In P. H. Abelson, Ed., *Researches in Geochemistry, Vol. 2,* p. 910–944. Wiley, New York.

Hodges, F. N. (1973) Solubility of H_2O in forsterite melt at 20 kbar. *Carnegie Inst. Wash. Year Book, 72,* 495–497.

Holloway, J. R. (1976) Fugacity and activity coefficients of molecular species in fluids at high pressures and temperatures. *Carnegie Inst. Wash. Year Book, 75,* 771–775.

——— (1977) Fugacity and activity of molecular species in supercritical fluids. In D. G. Fraser, Ed., *Thermodynamics in Geology,* p. 161–181. Reidel, Dordrecht, Holland.

Huang, W. L. and P. J. Wyllie (1976) Melting relationships in the systems CaO–CO_2 and MgO–CO_2 to 33 kbar. *Geochim. Cosmochim. Acta, 40,* 129–132.

Irving, A. J. and P. J. Wyllie (1975) Subsolidus and melting relationships for calcite, magnesite, and the join $CaCO_3$–$MgCO_3$ to 36 kbars. *Geochim. Cosmochim. Acta, 39,* 35–53.

Kennedy, G. C., G. J. Wasserburg, H. C. Heard and R. C. Newton (1962) The upper three-phase region in the system SiO_2–H_2O. *Am. J. Sci., 260,* 501–521.

Kerrick, D. M. (1974) Review of metamorphic mixed volatile (H_2O–CO_2) equilibria. *Am. Mineral., 59,* 729–762.

——— and J. Slaughter (1976) Comparison of methods for calculating and extrapolating equilibria in P–T–X_{CO_2} space. *Am. J. Sci., 276,* 883–916.

Mysen, B. O. and A. L. Boettcher (1975a) Melting of a hydrous mantle. I. Phase relations of natural peridotite at high pressures and temperatures with controlled activities of water, carbon dioxide, and hydrogen. *J. Petrol., 16,* 520–548.

——— and ——— (1975b) Melting of a hydrous mantle. II. Geochemistry of crystals and liquids formed by anatexis of mantle peridotite at high pressures and temperatures as a function of controlled activities of water, hydrogen, and carbon dioxide. *J. Petrol., 16,* 549–592.

———, D. H. Eggler, M. G. Seitz and J. R. Holloway (1976) Carbon dioxide in silicate melts and crystals, I. Solubility measurements. *Am. J. Sci., 276,* 455–479.

——— and M. G. Seitz (1975) Trace element partitioning determined by beta track mapping: an experimental study using carbon and samarium as examples. *J. Geophys. Res., 80,* 2627–2635.

Nakamura, Y. and I. Kushiro (1974) Composition of the gas phase in Mg_2SiO_4–SiO_2–H_2O at 15 kbar. *Carnegie Inst. Wash. Year Book, 73,* 255–258.

Nehru, G. E. and P. J. Wyllie (1975) Compositions of glasses from St. Paul's peridotite partially melted at 20 kbar. *J. Geol., 83,* 455–471.

Ricci, J. E. (1951) *The Phase Rule and Heterogeneous Equilibrium.* Dover Publications, New York.

Robie, R. A. and D. R. Waldbaum (1968) Thermodynamic properties of minerals and related substances at 298.15°K (25.0°C) and one atmosphere (1.013 bars) pressure and at higher temperatures. *U.S. Geol. Surv. Bull. 1259.*

Stewart, D. B. (1967) Four-phase curve in the system $CaAl_2Si_2O_8$–SiO_2–H_2O between 1 and 10 kbar. *Schweiz. Mineral. Petrogr. Mitt., 47,* 35–59.

Warner, R. D. (1973) Liquidus relations in the system CaO–MgO–SiO_2–H_2O at 10 kbar P_{H_2O} and their petrologic significance. *Am. J. Sci., 273,* 925–946.

Wyllie, P J. (1978) Mantle fluid compositions buffered in peridotite–CO_2–H_2O by carbonates, amphibole, and phlogopite. *J. Geol., 86,* 687–713.

——— and J. L. Haas, Jr. (1965) The system CaO–SiO_2–CO_2–H_2O: 1. Melting relationships with excess vapor at 1 kbar pressure. *Geochim. Cosmochim. Acta, 29,* 871–892.

——— and W. L. Huang (1975) High CO_2 solubilities in mantle magmas. *Geology, 4,* 21–24.

——— and ——— (1976) Carbonation and melting reactions in the system CaO–MgO–SiO_2–CO_2 at mantle pressures with geophysical and petrological applications. *Contrib. Mineral. Petrol., 54,* 79–107.

Manuscript received, April 9, 1979;
accepted for publication, January 15, 1980.